Spatiotemporal Variation of Flash Floods in the Hengduan Mountains Region Affected by Rainfall Properties and Land-use

Xiaoyun Sun
Institute of Geographic Sciences and Natural Resources Research CAS: Institute of Geographic Sciences and Natural Resources Research Chinese Academy of Sciences

Guotao Zhang
Institute of Mountain Hazards and Environment Chinese Academy of Sciences

Jiao Wang (wangjiao@imde.ac.cn)
Institute of Mountain Hazards and Environment Chinese Academy of Sciences

Chaoyue Li
Institute of Geographic Sciences and Natural Resources Research CAS: Institute of Geographic Sciences and Natural Resources Research Chinese Academy of Sciences

Shengnan Wu
Institute of Geographic Sciences and Natural Resources Research CAS: Institute of Geographic Sciences and Natural Resources Research Chinese Academy of Sciences

Yao Li
Institute of Mountain Hazards and Environment Chinese Academy of Sciences

Research Article

Keywords: Flash floods, Spatiotemporal variation, Rainfall, Land-use, The Hengduan Mountains region

Posted Date: June 4th, 2021

DOI: https://doi.org/10.21203/rs.3.rs-561906/v1

Version of Record: A version of this preprint was published at Natural Hazards on October 30th, 2021. See the published version at https://doi.org/10.1007/s11069-021-05061-5.

Spatiotemporal variation of flash floods in the Hengduan Mountains region affected by rainfall properties and land-use

Xiaoyun Sun[1,4], Guotao Zhang[2,4], Jiao Wang[2,3,*], Chaoyue Li[1,4], Shengnan Wu[1,4], Yao Li[1,4]

Abstract: Understanding the spatiotemporal characteristic of flash floods is significant for the reasonable and accurate identification of high-risk regions of disasters as well as future prediction of hydrological regimes. Therefore, this study collected time-series datasets (1979-2015) of historical flash flood events, rainfall, and land-use in the Hengduan Mountains region, China to characterize the spatiotemporal variation in flash floods affected by the change in rainfall and land-use. Using linear trend, a significant increase with 12 times/10a for flash flood events was found while 82% of events occurred in the flood season (June–August). They were closely related to the increase in frequency (3.5 d/10a) and magnitude (215.55 mm/10a) of heavy rainfall as well as the amplified artificial (999 km^2). Affected by heavy rainfall due to climate change and human activity, significant periodic

* Jiao Wang
wangjiao@imde.ac.cn

[1] Key Laboratory of Land Surface Pattern and Simulation, Institute of Geographic Sciences and Natural Resources Research, Chinese Academy of Sciences, Beijing 100101, China

[2] Key Laboratory of Mountain Hazards and Surface Process, Institute of Mountain Hazards and Environment, Chinese Academy of Sciences (CAS), Chengdu 610041, China

[3] China-Pakistan Joint Research Center on Earth Sciences, CAS-HEC, Islamabad 45320, Pakistan.

[4] University of Chinese Academy of Sciences, Beijing 100049, China

variations on the scales of 3-7a, 8-15a, and 21-31a were derived based on the Morlet wavelet analysis. Meanwhile, utilizing the standard elliptical difference, we identified the moving route of the gravity center of flash floods, with the direction from northwest to southeast. More recorded disasters generally were found in the south of the Hengduan Mountain region, where was mainly controlled by frequent rainstorms and the formation of more cropland and artificial with higher runoff potential. These findings can be an appropriate supplement for lack of understanding of the spatiotemporal dynamics of flash floods in the Hengduan Mountains region and could provide policymakers with evidence to identify high-risk areas which is difficult to cope with in the mountainous watershed.

Keywords: Flash floods; Spatiotemporal variation; Rainfall; Land-use; The Hengduan Mountains region

HIGHLIGHTS

- Spatiotemporal variation of flash flood events (FFE) in the Hengduan Mountains region (HMR) is characterized based on the recorded 1979-2015 events datasets.
- A significant increase with 12 times/10a for FFE is found due to heavy rainfall and the amplified artificial related to climate change and human activity.
- Significant periodic variations on the scales of 3-7a, and 8-15a for FFE are derived.
- The high-risk regions of flash flood disasters were identified in the south of the HMR.

1 Introduction

Flash floods, one of the deadliest natural hazards worldwide (Špitalar et al., 2014), generally result in loss of life and substantial economic damage (Kumar et al., 2018; Saharia et al., 2017; Yu et al., 2018b). Despite the global scale of flash floods happened, the suffering caused by flash floods remains unevenly distributed between different regions. For example, Asia and the Pacific are most afflicted compared to any other area of the world, account for over 90% of global disasters and upward trends of flash flood occurrences and impacts (Atif et al., 2021; Kimuli et al., 2021; Singh and Kumar, 2013). China, a mountainous country covering 2/3 of its area, is most threatened by flash floods with more than 60 000 events during 1949-2015(Yuan et al., 2017). The frequency and mortality of flash floods are the largest in Asia (Hu et al., 2018), and present a significant spatiotemporal disparity due to the complex monsoon climate and diverse geomorphological types (He et al., 2017; Liu et al., 2018; Liu et al., 2017).

Land-use and climate change are often referred to as 'global change' (Lopez-Tarazon et al., 2019), are two of the most critical drivers of hydrological variations (Kim et al., 2013; Kundu et al., 2017), affecting the formation and development of flash floods due to a complex interaction of the water-vegetation-soil system (Swain et al., 2021; Wang et al., 2020; Zhang et al., 2018). The weather system is becoming more and more unstable under climate change, increasing extreme weather events (Roy et al., 2020; Yu et al., 2018a). One of the main impacts appears to increase the frequency and

magnitude of extreme rainfall events (Allan and Soden, 2008; Barredo, 2006; Debortoli et al., 2017; Li et al., 2021; Llasat et al., 2021). Meanwhile, Land-use has undergone tremendous transition due to urbanization and the intensification of human activities (Antonio et al., 2019; Avashia and Garg, 2020; Wan Mohtar et al., 2020). Flash floods susceptibility in many regions is particularly heightened due to changing frequencies and magnitudes of extreme rainfall or land-use changes, particularly affected by a large urban growth (Borga et al., 2010; Llasat et al., 2016; Penna and Borga, 2013). Therefore, the increase in flash floods caused by the change in rainfall and land-use has attracted worldwide attention. It was quantitatively assessed that the impact of climate and land-use changes on the streamflow variations (Bronstert et al., 2002; Shahid et al., 2017; Swain et al., 2021), the discharges of the watershed with size from10 km^2 to 201 km^2 increased 185-560 m/s^3 from the baseline land-use to the urbanized in the Mediterranean by Antonio et al. (Antonio et al., 2019). And it was demonstrasted that a increasing trend of flash floods due to the rainfall and land-use variation (Llasat et al., 2014; Zhang et al., 2019b), the risk of flash floods in the Yesanpo Scenic Area of, Beijing, China, which has increased by 28% due to the development of tourism and land-use change (Chen et al., 2020).

As a 'natural laboratory' of climate change in China and even the world, the Tibetan Plateau is very sensitive to climate change (Cui et al., 2014; Cui et al., 2015; Yang et al., 2020). The Hengduan Mountains region (HMR), located in the eastern margin of the Tibetan Plateau, also has an obvious response to climate change (Wang et al., 2013; Xu et al., 2018), with an increase in extreme precipitation (Huang et al., 2020; Shi et al.,

2014; Wu et al., 2017; Zhang et al., 2014). Heavy rainfall distribution was affected by the complex topography and presented a significant spatial discrepancy (Li et al., 2021; Li et al., 2011; Ma et al., 2013). The morphology of the mountainous basins with small and steep river catchments can turn the intense runoff generation into severe devastating flash floods (Penna and Borga, 2013). Besides, the HMR has experienced dramatic land-use alterations over the past 20 years (Wang et al., 2018), but the effects of these changes on flash floods remain small. Additionally, the active strong earthquakes, frequent extreme rainfall events, and intensive artificial of major projects (such as the Sichuan-Tibet Railway) in the HMR severely affect the drastic hydrological changes in the Mountainous area, possibly leading to the increasing of the risk of flash floods (Zhang et al., 2021a; Zhang et al., 2019a).

It is essential to conduct comprehensive documentation of past events for flash flood research (Wang et al., 2020). Many researchers have been shown to collect history flash flood events and create the events database (Gaume et al., 2009), and being intensively studies of using the events, thus investigating frequency, temporal evolution, spatial distribution and patterns, fatalities, and injuries, as well as the seasonality of flash floods (Kaiser et al., 2021; Llasat et al., 2014), and analyzing the influence of environmental factors on the distribution of flash floods (Wang et al., 2020; Xiong et al., 2019). Also, the models were used to predict flash floods in the future (Avashia and Garg, 2020; Zhang et al., 2021b). However, there was a lack of synchronous analysis of the long-term spatiotemporal evolution of flash floods with rainfall and land-use due to the constraints of recorded data.

Therefore, this study selected the HMR, China, and collected time-series datasets (1979-2015) of historical flash flood events, rainfall, and land-use. The objectives of this study are to (1) characterize the spatiotemporal variability in flash floods during 1979-2015 in the HMR, and (2) exploit the effects of rainfall properties and land-use on the spatiotemporal characteristics of flash floods. They could provide scientific reference and decision-making for formulating reasonable measures of disaster prevention and mitigation, as well as effective flood risk management.

2 Materials and Methods

2.1 Study area

The HMR (24°39′N~33°34′N, 96°58′E~104°27′E) is located in southwest China. It belongs to the transition area between Tibetan Plateau and Sichuan Basin; the elevation decreases from northwest to southeast (Fig. 1). The neotectonic movement is active and the terrain is steep under the control of the uplift and orogeny of the Tibetan Plateau. Within a horizontal distance of 70-150 km from east to west, the vertical height difference is about 4 000 m, and the terrain gradient is up to 2%-6%. The HMR is a typical monsoon climate area, which is influenced not only by the East Asian monsoon from the Western Pacific Ocean but also by the South Asian monsoon from the Bay of Bengal and the Indian Ocean as well as by the Tibetan Plateau monsoon and westerlies. Influenced by various monsoons and complex terrain, the Mountainous area presents prominent seasonal and vertical climatic zones (Yu et al., 2018a). Under the influence of climate change and the strength and retreat of the monsoon, burdensome rain events frequently occur (Kumar et al., 2018; Li et al., 2012).

The significant difference in climate conditions between different regions contributes to various vegetation types (Yin et al., 2020), including shrub, forest, and meadows.

Fig. 1 The HMR with meteorological stations and locations of flash flood events

2.2 Data preparation

2.2.1 Flash flood events

The flash flood events data are mainly from the database of the "National Flash Flood Investigation and Evaluation Project" of China Institute of Water Resources and Hydropower Research, including the records of more than 60,000 flash flood events of China from 1950 to 2015, as well as the occurrence time, location, precipitation and injuries of the disaster events. In consideration of incomplete records in the early period, the data of 2044 flash flood events in the HMR from 1979 to 2015 were selected in this study.

2.2.2 Rainfall

Daily precipitation data, including meteorological station data and grid data, were used to analyze the spatiotemporal evolution of rainfall in the HMR. The meteorological station data were acquired by national standard meteorological stations in the HMR, and 25 stations were selected based on their record length with flash floods data—the data obtained from the China Meteorological Data Network (http://data.cma.cn). The grid data is CPC Global Unified Gauge-Based Analysis of Daily Precipitation (0.50 - degree latitude × 0.50 - degree longitude grid), which is part of products suite from the Unified Precipitation Project that is underway at the National Oceanic and Atmospheric Administration (NOAA) Climate Prediction

Center (CPC), available from https://psl.noaa.gov/.

Rainfall events are often classified in terms of depth of rain deliver in 24 hours (Breugem et al., 2020), in this respect, mentions heavy rainfall defined as daily precipitation greater than or equal to 50 mm, and the rainstorm days is the number of days in which a heavy rainfall event occurs. This indicator is not only a "climate change indices" (http://etccdi.pacificclimate.org/list_27_indices.shtml) used by the World Meteorological Organization Climate Commission for Climatology (WMO-CCI), and widely used rainstorm classification standard in China (Li et al., 2019; Zhang et al., 2014; Zhou et al., 2011). At the same time, this threshold is also the critical value for the warning of mountain disasters in the region (Li et al., 2019).

2.2.3 Land-use

This study used land-use data (1 km resolution) from Resource and Environment Science and Data Center of Chinese Academy of Sciences (http://www.resdc.cn/), which provides land-use data at 5-year or 10-year intervals from 1980 to 2015 in six classes: cropland, forest, grass, water, artificial, and unused land.

2.3 Methods

2.3.1 Linear trend and Wavelet analysis

The changing trend of flash floods and rainfall is expressed by a linear equation (Mudelsee, 2019; Xu et al., 2018), that is:

$$y = a + bt \tag{1}$$

where y is flash flood events and rainfall, t is time (the time is 1979-2015 in this study), b is the linear trend term.

Wavelet analysis (Teresa and Gabriele, 2020) is an effective method for signal processing and has been widely used in the time-frequency analysis of rainfall series. Morlet wavelet function is a kind of complex-valued wavelet that is widely used for systematic analysis. Its expression is as follows:

$$\varphi(t) = e^{ict} g e^{-t^2/2} \tag{2}$$

where i is a complex, c is a constant.

For a given discrete time series $f(k\Delta t)$ ($k = 1, 2, \mathrm{K}, N$; Δt is the sampling interval), and its wavelet transform is

$$W_f(a,b) = |a|^{-1/2} \sum_{k=1}^{N} f(k) g e^{ict} e^{-t^2/2} \tag{3}$$

where a is the period length of the wavelet; b is the time shift of the wavelet; $W_f(a,b)$ is the wavelet transform coefficient.

On this basis, the wavelet square difference is calculated, namely:

$$var = \int_{-\infty}^{\infty} \left| W_f(a,b) \right|^2 db \tag{4}$$

equation (3) is used to calculate the wavelet variance and draw the wavelet variance graph, the main period of time-series can be determined.

2.3.2 Gravity center model and standard deviation ellipse

The gravity center (mean center) was used to systematically analyze the historical flash flood events and rainfall in the HMR from 1979 to 2015. According to the moving track and distance of disasters center in ten years, the directional distribution of disasters was analyzed in combination with the standard deviation ellipse (Xiong et al., 2019). The standard deviational ellipse is used to identify the spatial distribution of historical flash flood events and to represent the location change

and movement trend of disasters center. The long axis of the standard deviational ellipse represents the directivity of the spatial distribution of flash floods. In contrast, the short axis represents the dispersion degree of the spatial distribution of the disasters.

The mean center is the average *x*- and *y*-coordinate of all the features in the study area. It's helpful in tracking changes in the distribution or for comparing the distributions of different types of components. The mean center is given as:

$$\overline{X} = \frac{\sum_{i=1}^{n} x_i}{n}, \overline{Y} = \frac{\sum_{i=1}^{n} y_i}{n} \tag{5}$$

where x_i and y_i are the coordinates for feature i, and n is equal to the total number of features.

The weighted mean center extends to the following:

$$\overline{X_w} = \frac{\sum_{i=1}^{n} w_i x_i}{\sum_{i=1}^{n} w_i}, \overline{Y_w} = \frac{\sum_{i=1}^{n} w_i y_i}{\sum_{i=1}^{n} w_i} \tag{6}$$

where w_i is the weight at feature i.

The standard deviational ellipse is used to identify the spatial distribution of historical flash floods and to represent the location change and movement trend of disasters center. The long axis of the standard deviational ellipse represents the directivity of the spatial distribution of disasters. In contrast, the short axis represents the dispersion degree of the spatial distribution of catastrophe.

The Standard Deviational Ellipse is given as:

$$SED_x=\sqrt{\frac{\sum_{i=1}^{n}\left(x_i-\overline{X}\right)^2}{n}},SED_y=\sqrt{\frac{\sum_{i=1}^{n}\left(y_i-\overline{Y}\right)^2}{n}} \quad (7)$$

where x_i and y_i are the coordinates for feature i, $\{\overline{X},\overline{Y}\}$ represent the mean center for features, and n is equal to the total number of the features.

The angle of rotation is calculated as:

$$tan\theta=\frac{A+B}{C} \quad (8)$$

$$A=\left(\sum_{i=1}^{n}\tilde{x}_i^2-\sum_{i=1}^{n}\tilde{y}_i^2\right) \quad (9)$$

$$B=\sqrt{\left(\sum_{i=1}^{n}\tilde{x}_i^2-\sum_{i=1}^{n}\tilde{y}_i^2\right)^2+4\left(\sum_{i=1}^{n}\tilde{x}_i^2\tilde{y}_i^2\right)^2} \quad (10)$$

$$C=2\sum_{i=1}^{n}\tilde{x}_i\tilde{y}_i \quad (11)$$

where $\tilde{x}_i$ and $\tilde{y}_i$ are the deviations of the *xy*-coordinates from the mean center.

4 Results

4.1 Temporal variation in flash floods

The interannual variability of flash floods in the HMR during 1979-2015 was analyzed with the undulant rising characteristic at 12 times/10a (Fig. 2a). There were two particular large flash flood events exceptions in 1991 (138 events) and 1998 (230 events) when the catastrophic floods were triggered by the monsoon rainfalls in the Yangtze River Basin, resulting in 4 150 people died and directed economic losses of RMB166 billion (Kundzewicz et al., 2020). Meanwhile, it was found that the monthly distribution of flash floods mainly occurred in summer from June to August, with the occupy 82.0 % (1594 events) of the whole year (Fig. 2b). The largest proportion

appeared in July with 670 occurrences, accounting for 34.8% of the total. This finding has been verified each year from 1979 to 2015, indicating the frequent month of flash flood disaster occurrence.

Fig. 2 The statistically annual variation (a) and monthly distribution (b) of flash floods in the HMR during 1979-2015

Additionally, the periodic changes of the time-series flash floods were identified based on the wavelet coefficients (Fig.3a), which could be used to predict the future change trend of the flash floods at different time scales. It can be seen that the potential periodicities with 3-7a, 8-15a, and 21-31a of the time-series flash floods from 1979 to 2015 (Fig. 3a) were obtained, and significant periodicity with the local higher energy density appeared in the periods of 3-7a and 8-15a. But the period of 21-31a with the weak energy was widely distributed in the periods from 1979 to 2015. Three prominent peaks were found in the wavelet deviation diagram (Fig. 3b), The fluctuation of three periods efficiently controlled the variation characteristics of flash floods during the time series of 1979-2015. The maximum value of the wavelet peak appeared in the period scale of 9 a when indicating the strongest periodic oscillation.

Fig.3 Distribution of time frequencies on the real part of wavelet transform (a) and the wavelet variances (b) in flash floods in the HMR during 1979-2015

4.2 Spatial distributions in flash floods

The historical flash flood events from 1979 to 2015 were counted with a 10-year interval. In different decades, the spatial moving track and distance of gravity center of flash floods were analyzed based on the gravity center model (Fig. 4), and the

disaster distribution and direction were comprehensively estimated using the standard deviation ellipse. The calculated critical parameters of gravity center and standard deviation elliptical were determined in Table.1, including coordinate and the movement distance of centroids, as well as direction angle and X, Y-axis distance of standard deviation elliptical. During the periods from 1979 to 2015, the region in the gravity center of flash floods was determined between 101.40°~101.59°E, 26.99°~28.03°N, located in Panzhihua City and Liangshan Yi Autonomous Prefecture, Sichuan province.

It was found that the gravity center mainly moved upward from northeast to southeast, first moving 74 km from north to south, then 3 km west, and finally 174 km northeast; The change of the direction angle was not significant, ranging from 3.44° to 174.13°. The flash floods presented a north-south pattern, and the pattern showed a trend of strengthening, strengthening, and weakening in turn. The length of the significant half axis along the X-axis showed a decreasing trend on the whole, and the data showed a high-low-high fluctuation, indicating that the directivity of the spatial distribution of flash floods first weakened and then increased. The north-south pattern changed from significant to non-significant and then to substantial. The average length of the short half axis along the Y-axis was 264 km. The short half axis of 1979-1985 was the longest, indicating that the centripetal force of the distribution of flash floods was weak and the dispersion degree of disasters was large.

Fig.4 Gravity Center and Directional Distribution of flash floods from 1979 to 2015

Table 1 The parameters of gravity center and standard deviation ellipse in different

decades from 1979 to 2015

4.3 Changes in rainfall characteristics and land-use

4.3.1 Rainfall characteristic

A decreasing trend of 10.48mm/10a for the average annual rainfall was found in the HMR, and the maximum value of precipitation appeared in 1998 (Fig. 5a). However, an increasing trend of 3.5d/10a for the number of rainstorm days and 255.6mm/10a for rainstorms precipitation was determined, and the peaks also occurred in 1998 (Fig. 5b, c). Additionally, the monthly rainfall depth and the number of rainstorm days varied significantly within the year, and both maximum values occurred in July (Fig. 5d). Especially, the rainstorm days and rainstorms precipitation from June to August accounted for 80% of the total of each year (Fig. 5e, f). The characteristic was parallel to the temporal variations in flash flood events. The annual distribution of precipitation shows clear seasonality, being strongly influenced by the monsoon.

Fig. 5 Annual evolution (a, b, c) and monthly distribution (d, e, f) of the rainfall (unit: mm), the rainstorm days (unit: d), and the rainstorms precipitation (unit: mm) in the HMR from 1979 to 2015

Three over-centers (i.e. 1886, 2006, 2014) and two under-centers (1979 and 2015) were obtained during the periods from 1979 to 2015. It can be seen from Fig.6a that during the evolution process of rainfall from 1979 to 2015, there was a certain periodicity on the scales of 3-8a, 9-17a, and 21-32a. In contrast, the energy density of 21-32a was relatively high, but the periodic variation was only significant from 1989

298 to 2011, while the other periodic time-domain was fairly broad but not significant. In
299 the wavelet square deviation graph (Fig. 6b), there were two fairly obvious peaks,
300 which correspond to the time scale of 22a and 28a successively from small to large.
301 The maximum peak corresponds to the time scale of 28a, indicating that the periodic
302 oscillation of about 28a was the strongest, which was the first main period of rainfall
303 variation. The 22a time scale corresponds to the second peak, which is the second
304 principal period.

305 **Fig. 6** Distribution of time frequencies on the real part of wavelet transform (a) and
306 the wavelet variances (b) in precipitations in the HMR during 1979-2015

307 The spatial distribution of rainfall in the HMR region was different, affected by
308 the topography (Li et al., 2021), which decreased from southwest to northwest (Fig.
309 7a-d). The rainy belt was in a 'NE-SW' direction, and the rainfall center moved in the
310 same order with a distance of 3.8-16.2 km during 1979-2015 (Fig. 7e). The maximum
311 precipitation occurred in the east-north-east direction of the study area, located in
312 Ya'an, Sichuan, a rainstorm center in Sichuan. The minimum of rain appears in the
313 west-north-west order of the study area, situated in Qamdo, Tibet. It is found that
314 heavy rainfall mainly occurs in areas with high precipitation, located in the lower
315 elevation of the south of the region where flash floods frequently occurred (Fig. 8).

316 **Fig. 7** Moving track of the rainfall center (1979-2015)

317 **Fig. 8** Distribution of the rainstorm days and rainstorm precipitation in
318 meteorological stations in the HMR (1979-2015)

319 **4.3.2 Land-use change**

320 The land-use maps in 1980-2015 were shown in Fig. 9, and the area of the
321 land-use in the different year was counted in Table. 2. It was evident that an apparent
322 spatial heterogeneity in land-use distribution. Forest and grass were the main land-use
323 types and were widely distributed in the mountainous, accounting for about 88%. The
324 grass was mainly concentrated in the north of the region with high altitude, while
325 forests in the middle and south with a low height. Other land-use types were scattered
326 and small in area (only 0.2%-7.7%). Artificial and cropland are mainly distributed in
327 the southeast of the mountains with lower elevation and concentrated in the river
328 valley due to the topography restriction. Unused land is distributed primarily in the
329 northwest of the region, which is primarily in Ganzi and Qamdo, while the water area
330 is primarily distributed in the middle.

331 From 1980 to 2015, following the urban development, the artificial expanded
332 rapidly (from 727 km^2 to 1726km^2), increasing to 137%. Before 2005, rampant
333 growth led to a significant reduction in forest and increased grass. Then in 2015, the
334 forest has recovered, increasing by 6 685 km^2 compare with 1980, while grass
335 decreased by 2 932 km^2. Besides, cropland, water area, and unused land decreased by
336 138 km^2, 2 284 km^2, and 927 km^2 respectively in the past 35 years.

337 **Fig. 9** The land-use maps in the HMR from 1980 to 2015 (km^2)

338 **Table 2** The area of land-use in the HMR during 1980-2015 (km^2)

339 The land-use maps of 1980 and 2015 were superimposed to obtain the transfer
340 area matrix, which was shown in Table.3. The land-use changed abruptly and
341 dramatically over the past 35 years in the HMR (Fig.10); in particular, more

incredible conversion among cropland, forest, the grass is noteworthy. The decrease in cropland is due to conversion to artificial, forest, and grass. The main reason for the decline of grass and the increase of forest is that a large area of grass (49 291 km^2) has been converted into the forest. These changes were closely related to national policies to protect the ecological environment, such as returning cropland to forest and grass and afforestation. Also, unused land has been turned into grass (1 557 km^2) and forest (6957 km^2), which shows that the ecology of the HMR has been improved. The increase of artificial mainly comes from the conversion of cropland (910 km^2) and grass (381 km^2). Due to the acceleration of urbanization driven by social and economic development, other land-use types are also being transformed into artificial. The conversion of land-use type to cropland and artificial is mainly in the south of the region, where the altitude is low and human activities are intense, while the conversion to forest and grass is primarily in the northern, especially in the northwest, which is primarily in the high-altitude mountainous areas.

Table 3 Land-use transfer matrix from 1980 to 2015 (km^2)

Fig. 10 Distribution of land-use transfer from 1980 to 2015

5 Discussion

5.1 Controls of rainfall properties to spatiotemporal variability in flash floods

The occurrence and distribution of flash floods are controlled by rainfall, which is the main trigger factor, and associated with short, high-intensity rain (Borga et al., 2010). The heavy rainfall over a short period causes quick-rising flash floods, which is very common (Roy et al., 2020). The contribution of convective precipitation was about

364 50% for 75% of the flash floods, and it increases to 70% for 50% of them (Llasat et al.,
365 2016). The HMR is one of the most affected regions, where convective activity bearing
366 severe weather and intense rainfall is favored due to the combination of the multiple
367 monsoons and the complex and accompanied by large spatial and decadal variability
368 (Yin et al., 2018). Flash floods directly linked to rainfall, this study indirectly analyzed
369 whether the magnitude of the trigger itself had also varied through space and time,
370 enabling considerations in the context of climatic changes. It was demonstrated that
371 the spatiotemporal variations of flash floods and triggering factor rainfall are highly
372 consistent.

373 The annual distribution of rainfall shows clear seasonality, being strongly
374 influenced by the monsoon (Wang et al., 2020; Yuan et al., 2017), mainly concentrated in
375 summer (June to August), and flash floods were highly similar to heavy rainfall
376 because the other factors of flash floods have slight annual variation. There was a
377 decrease in the precipitation (10.48mm/10a), but an increase in days (3.5 d/10a) and
378 precipitation (215.55 mm/10a) of heavy rainfall events under climate change. The
379 increasing trend of flash floods (12times/10a) was more dramatic than the rainstorms,
380 which may be due to the synergistic effect of the increase in frequency and magnitude
381 of rainstorms (Fig. 11), triggering more flash floods in a rainstorm event. It may also
382 be affected by land-use changes that increase flash flood sensitivity. In addition, it is
383 worth noting that the relationship between flash floods period and rainfall period has
384 been found in this study. The resonance period on the same scales of 3-7a, 21-31a
385 appears in the evolution of flash floods and rainfall during the time series of

1979-2015, and they were controlled by the same period with 22a.

Fig. 11 Number of flash floods under different rainfall grades

The distribution pattern of rainfall or extreme heavy rainfall usually had a high consistency with regional topographical changes (del Moral et al., 2020; Li et al., 2021). The spatial distribution of flash floods is more in the south and less in the north, and the least in the northwest, which was similar to the spatial distribution of rainfall and rainstorms. Comparison of gravity center migration trajectory of rainfall and flash floods, the results show that, from 1979-1985 to 1986-1995, the gravity centers of rainfall and flash floods do not overlap. Still, there was a remarkable correlation between the migration trajectory of the gravity center of precipitation and flash floods in the direction of longitude, which is mainly from north to south. From 1986-1995 to 1996-2005, the gravity center of flash floods migrates westward, while the gravity center of rainfall migrates southwest, which may be due to two heavy rainfall events (the 1991 and 1998 floods) in the southeast of the area during this period. From 1996-2005 to 2006-2015, the gravity centers migrated in very similar directions, from southwest to northeast. These indicate an excellent correlation between the trajectory of flash floods gravity center and the trajectory of precipitation gravity center in the direction, and the occurrence of flash floods is greatly affected by the change of rainfall. At the same time, other factors are affecting the occurrence of flash floods. These results indicated that the spatiotemporal evolution of flash floods is predominantly influenced by rainfall changes in the HMR, subject to climate change.

5.2 Effects of land-use on the spatiotemporal characteristic in flash floods

Land-use change directly impacts the underlying surface of the drainage basin, generally altered the runoff generation and confluence processes at hillslopes (Elfert and Bormann, 2010), furtherly affecting the formation and development of flash floods in the watershed. It was demonstrated that the sensitivity of flash floods increased in artificial and cropland while decreased in forests and grass (Yue et al., 2016).

Forest and grass could intercept rainfall and regulate runoff, efficiently lowering the peak discharge and delay the peak time of flash floods. In contrast, the frequency of flash floods was higher in artificial and cropland (He et al., 2005; Yue et al., 2016). For example, in the Chabagou catchment with 205 km^2, Shaanxi Province, China, the grass and forest could decrease flood peaks by 36% and 64%, respectively (Fu et al., 2020). In the middle and northwestern of the HMR, large land-use areas have been converted to forest and grass, which can effectively alleviate flash floods, so flash floods were less frequent in this region (Fig. 10). However, due to the destruction of vegetation-soil at cropland and irrigation, can moisten the soil, thus contributing to both precipitation and runoff intensification, it is very extreme to cause flash floods accompanied by soil erosion (Fu et al., 2020; O'Donnell et al., 2011). The small area of cropland only accounts for 7.7%, 31.9% of flash floods occurred in the HMR. High surface runoff from heavy rainfall due to the impervious surfaces and high building densities of artificial, the hydrological response changed to higher flow rate peaks and shorter concentration times, escalate the urban flooding (Antonio et al., 2019; Wan Mohtar et al., 2020). Chen analyzed the risk of flash floods in the Yesanpo Scenic Area of Beijing, China, which has increased by 28% due to tourism and land-use alteration

(Chen et al., 2020). The smallest area of artificial could trigger the largest probability of flash floods, accounting for only 0.8% of the mountain area, but 4.9% of flash floods occurred. In the south of the HMR, with low altitude and intense human activities, most of the cropland and artificial was distributed. A large of land-use has been altered into them, which is a susceptible area of flash floods. This indicates the effect of the pattern of land-use change on the spatiotemporal evolution of flash floods in the HMR.

6. Conclusions

The spatiotemporal variation in flash floods with 2044 events during 1979-2015 in the HMR with high relief were characterized based on linear trend, wavelet analysis, gravity center model, and standard deviational ellipse. A significant increase with 12 times/10a for flash flood events during the periods was found due to the high frequency and magnitude of heavy rainfall and the amplified artificial. It was noted that historical events were characterized by significant periodicities (3-7a, 8-15a, and 21-31a), which were subject to changes in rainstorm extremes affected by climate change and human activity.

Meanwhile, affected by the spatial distribution of heavy rainfall as well as expansion of cropland and artificial, the spatial gravity center of flash floods, during 1979-2015, gradually migrates along the direction from northwest to southeast. Higher frequencies of flash flood events generally appeared in the south region of the HMR, indicating the uneven spatiotemporal distribution of flash flood events. These findings could provide governments' policymakers with reasonable identification and

future prediction of high-risk regions of the considerable flash floods in the HMR under the future global change scenarios.

Declaration of competing interest

The authors declare that they have no known competing financial interests or personal relationships that could have appeared to influence the work reported in this paper.

Acknowledgments

This work was jointly supported by the Major Program of National Natural Science Foundation of China (Grant numbers 41790432 and 41941017); the Strategic Priority Research Program of the Chinese Academy of Sciences (Grant number XDA23090303).

Author contributions

Xiaoyun Sun: Conceptualization, Methodology, Software, Writing. **Guotao Zhang:** Conceptualization, Supervision, Writing - review & editing. **Jiao Wang:** Supervision, Funding acquisition. **Chaoyue Li:** Conceptualization, Software. **Shengnan Wu:** Writing - review & editing. **Yao Li:** Methodology, Software.

Declaration of interests

☒ The authors declare that they have no known competing financial interests or personal relationships that could have appeared to influence the work reported in this paper.

☐The authors declare the following financial interests/personal relationships which may be considered as potential competing interests:

References

Allan RP and Soden BJ (2008) Atmospheric warming and the amplification of precipitation extremes. Science, 321(5895): 1481-1484. http://dx.doi.org/10.1126/science.1160787

Antonio JA, Javier VA, Pla C et al. (2019) Impact of land use changes on flash flood prediction using a sub-daily SWAT model in five Mediterranean ungauged watersheds (SE Spain). Sci Total Environ, 657: 1578-1591. http://dx.doi.org/10.1016/j.scitotenv.2018.12.034

Atif S, Umar M and Ullah F (2021) Investigating the flood damages in Lower Indus Basin since 2000: Spatiotemporal analyses of the major flood events. Natural Hazards. http://dx.doi.org/10.1007/s11069-021-04783-w

Avashia V and Garg A (2020) Implications of land use transitions and climate change on local flooding in urban areas: An assessment of 42 Indian cities. Land Use Policy, 95: 104571. http://dx.doi.org/10.1016/j.landusepol.2020.104571

Barredo JI (2006) Major flood disasters in Europe: 1950–2005. Natural Hazards, 42(1): 125-148. http://dx.doi.org/10.1007/s11069-006-9065-2

Borga M, Anagnostou EN, Blöschl G et al. (2010) Flash floods: Observations and analysis of hydro-meteorological controls. Journal of Hydrology, 394(1-2): 1-3. http://dx.doi.org/10.1016/j.jhydrol.2010.07.048

Breugem AJ, Wesseling JG, Oostindie K et al. (2020) Meteorological aspects of heavy

precipitation in relation to floods – An overview. Earth-Science Reviews, 204: 103171. http://dx.doi.org/10.1016/j.earscirev.2020.103171

Bronstert A, Niehoff D and Bürger G (2002) Effects of climate and land-use change on storm runoff generation: present knowledge and modelling capabilities. Hydrological Processes, 16(2): 509-529. http://dx.doi.org/10.1002/hyp.326

Chen Y, Wang Y, Zhang Y et al. (2020) Flash floods, land-use change, and risk dynamics in mountainous tourist areas: A case study of the Yesanpo Scenic Area, Beijing, China. International Journal of Disaster Risk Reduction, 50: 103171. http://dx.doi.org/https://doi.org/10.1016/j.ijdrr.2020.101873

Cui P, Chen R, Xiang L et al. (2014) Risk Analysis of mountain hazards in Tibetan Plateau under global warming Climate Change Research, 10(2): 103-109.

Cui P, Su F, Zou Q et al. (2015) Risk assessment and disaster reduction strategies for mountainous and meteorological hazards in Tibetan Plateau. Chinese Science Bulletin, 60(32): 3067-3077. http://dx.doi.org/10.1360/n972015-00849

Debortoli NS, Camarinha PIM, Marengo JA et al. (2017) An index of Brazil's vulnerability to expected increases in natural flash flooding and landslide disasters in the context of climate change. Natural Hazards, 86(2): 557-582. http://dx.doi.org/10.1007/s11069-016-2705-2

del Moral A, Llasat MdC and Rigo T (2020) Connecting flash flood events with radar-derived convective storm characteristics on the northwestern Mediterranean coast: knowing the present for better future scenarios adaptation. Atmospheric Research, 238: 104863. http://dx.doi.org/10.1016/j.atmosres.2020.104863

521 Elfert S and Bormann H (2010) Simulated impact of past and possible future land use
522 changes on the hydrological response of the Northern German lowland 'Hunte'
523 catchment. Journal of Hydrology, 383(3-4): 245-255.
524 http://dx.doi.org/10.1016/j.jhydrol.2009.12.040
525 Fu S, Yang Y, Liu B et al. (2020) Peak flow rate response to vegetation and terraces
526 under extreme rainstorms. Agriculture, Ecosystems & Environment, 288: 106714.
527 http://dx.doi.org/10.1016/j.agee.2019.106714
528 Gaume E, Bain V, Bernardara P et al. (2009) A compilation of data on European flash
529 floods. Journal of Hydrology, 367(1-2): 70-78.
530 http://dx.doi.org/10.1016/j.jhydrol.2008.12.028
531 He B, Huang X, Ma M et al. (2017) Analysis of flash flood disaster characteristics in
532 China from 2011 to 2015. Natural Hazards, 90(1): 407-420.
533 http://dx.doi.org/10.1007/s11069-017-3052-7
534 He Y, Ma Z, Xie H et al. (2005) Mountain hazards intergrated senstivity on land use
535 of the upper reaches of Yangtza River--A case study of Xiaojiang River Basin.
536 Resources and Environment in the Yangtze Basin, 14(4): 528-533.
537 Hu P, Zhang Q, Shi P et al. (2018) Flood-induced mortality across the globe:
538 Spatiotemporal pattern and influencing factors. Sci Total Environ, 643: 171-182.
539 http://dx.doi.org/10.1016/j.scitotenv.2018.06.197
540 Huang C, Li G, Zhang F et al. (2020) Evolution characteristics of mountain
541 rainstorms over Sichuan Province in the past ten years under the influence of
542 climate change. Torrential Rain and Disasters, 39(4): 335-343.

543 http://dx.doi.org/10.3969/j.issn.1004-9045.2020.04.003
544 Kaiser M, Günnemann S and Disse M (2021) Spatiotemporal analysis of heavy
545 rain-induced flood occurrences in Germany using a novel event database
546 approach. Journal of Hydrology, 595: 125985.
547 http://dx.doi.org/10.1016/j.jhydrol.2021.125985
548 Kim J, Choi J, Choi C et al. (2013) Impacts of changes in climate and land use/land
549 cover under IPCC RCP scenarios on streamflow in the Hoeya River Basin, Korea.
550 Sci Total Environ, 452-453: 181-95.
551 http://dx.doi.org/10.1016/j.scitotenv.2013.02.005
552 Kimuli JB, Di B, Zhang R et al. (2021) A Multisource Trend Analysis of Floods in
553 Asia-Pacific 1990 – 2018: Implications for Climate Change in Sustainable
554 Development Goals. International Journal of Disaster Risk Reduction, 59: 102237.
555 http://dx.doi.org/10.1016/j.ijdrr.2021.102237
556 Kumar A, Gupta AK, Bhambri R et al. (2018) Assessment and review of
557 hydrometeorological aspects for cloudburst and flash flood events in the third
558 pole region (Indian Himalaya). Polar Science, 18: 5-20.
559 http://dx.doi.org/10.1016/j.polar.2018.08.004
560 Kundu S, Khare D and Mondal A (2017) Individual and combined impacts of future
561 climate and land use changes on the water balance. Ecological Engineering, 105:
562 42-57. http://dx.doi.org/10.1016/j.ecoleng.2017.04.061
563 Kundzewicz ZW, Huang J, Pinskwar I et al. (2020) Climate variability and floods in
564 China - A review. Earth-Science Reviews, 211: 103434.

565 http://dx.doi.org/10.1016/j.earscirev.2020.103434
566 Li G, Yu Z, Wang W et al. (2021) Analysis of the spatial Distribution of precipitation
567 and topography with GPM data in the Tibetan Plateau. Atmospheric Research,
568 247: 105259. http://dx.doi.org/10.1016/j.atmosres.2020.105259
569 Li Q, Wang Y, Xu P et al. (2019) Changes of extreme precipitation patterns for
570 disaster prone areas in the north of the Hengduan Mountains under climate
571 change. Mountain Resarch 37(3): 400-408.
572 Li Z, He Y, Wang C et al. (2011) Spatial and temporal trends of temperature and
573 precipitation during 1960–2008 at the Hengduan Mountains, China. Quaternary
574 International, 236(1-2): 127-142. http://dx.doi.org/10.1016/j.quaint.2010.05.017
575 Li Z, He Y, Wang P et al. (2012) Changes of daily climate extremes in southwestern
576 China during 1961–2008. Global and Planetary Change, 80-81: 255-272.
577 http://dx.doi.org/10.1016/j.gloplacha.2011.06.008
578 Liu Y, Yang Z, Huang Y et al. (2018) Spatiotemporal evolution and driving factors of
579 China's flash flood disasters since 1949. Science China Earth Sciences, 61(2):
580 1804–1817. http://dx.doi.org/10.1360/n072017-00328
581 Liu Y, Yuan X, Guo L et al. (2017) Driving Force Analysis of the Temporal and
582 Spatial Distribution of Flash Floods in Sichuan Province. Sustainability, 9(9):
583 1527. http://dx.doi.org/10.3390/su9091527
584 Llasat MC, del Moral A, Cortès M et al. (2021) Convective precipitation trends in the
585 Spanish Mediterranean region. Atmospheric Research.
586 http://dx.doi.org/10.1016/j.atmosres.2021.105581

587 Llasat MC, Marcos R, Llasat-Botija M et al. (2014) Flash flood evolution in
588 North-Western Mediterranean. Atmospheric Research, 149: 230-243.
589 http://dx.doi.org/10.1016/j.atmosres.2014.05.024
590 Llasat MC, Marcos R, Turco M et al. (2016) Trends in flash flood events versus
591 convective precipitation in the Mediterranean region: The case of Catalonia.
592 Journal of Hydrology, 541: 24-37. http://dx.doi.org/10.1016/j.jhydrol.2016.05.040
593 Lopez-Tarazon JA, Bronstert A, Thieken AH et al. (2019) The effects of global
594 change on floods, fluvial geomorphology and related hazards in mountainous
595 rivers. Sci Total Environ, 669: 7-10.
596 http://dx.doi.org/10.1016/j.scitotenv.2019.03.026
597 Ma Z, Liu J, Zhang S et al. (2013) Observed Climate Changes in Southwest China
598 during 1961–2010. Advances in Climate Change Research, 4(1): 30-40.
599 http://dx.doi.org/10.3724/sp.J.1248.2013.030
600 Mudelsee M (2019) Trend analysis of climate time series: A review of methods.
601 Earth-Science Reviews, 190: 310-322.
602 http://dx.doi.org/10.1016/j.earscirev.2018.12.005
603 O'Donnell G, Ewen J and O'Connell PE (2011) Sensitivity maps for impacts of land
604 management on an extreme flood in the Hodder catchment, UK. Physics and
605 Chemistry of the Earth, Parts A/B/C, 36(13): 630-637.
606 http://dx.doi.org/10.1016/j.pce.2011.06.005
607 Penna D and Borga M (2013) Natural Hazards Assessment in Mountainous Terrains
608 of Europe, Climate Vulnerability, pp. 229-239.

609 Roy P, Chandra Pal S, Chakrabortty R et al. (2020) Threats of climate and land use
610 change on future flood susceptibility. Journal of Cleaner Production, 272: 122757.
611 http://dx.doi.org/10.1016/j.jclepro.2020.122757
612 Saharia M, Kirstetter P-E, Vergara H et al. (2017) Characterization of floods in the
613 United States. Journal of Hydrology, 548: 524-535.
614 http://dx.doi.org/10.1016/j.jhydrol.2017.03.010
615 Shahid M, Cong Z and Zhang D (2017) Understanding the impacts of climate change
616 and human activities on streamflow: a case study of the Soan River basin,
617 Pakistan. Theoretical and Applied Climatology, 134(1-2): 205-219.
618 http://dx.doi.org/10.1007/s00704-017-2269-4
619 Shi P, Sun S, Wang M et al. (2014) Climate change regionalization in China (1961–
620 2010). Science China Earth Sciences, 44: 2294-2306.
621 Singh O and Kumar M (2013) Flood events, fatalities and damages in India from 1978
622 to 2006. Natural Hazards, 69(3): 1815-1834.
623 http://dx.doi.org/10.1007/s11069-013-0781-0
624 Špitalar M, Gourley JJ, Lutoff C et al. (2014) Analysis of flash flood parameters and
625 human impacts in the US from 2006 to 2012. Journal of Hydrology, 519: 863-870.
626 http://dx.doi.org/10.1016/j.jhydrol.2014.07.004
627 Swain SS, Mishra A, Chatterjee C et al. (2021) Climate-changed versus land-use
628 altered streamflow: A relative contribution assessment using three complementary
629 approaches at a decadal time-spell. Journal of Hydrology, 596: 126064.
630 http://dx.doi.org/10.1016/j.jhydrol.2021.126064

631 Teresa PC and Gabriele C (2020) Intra-catchment comparison and classification of
632 long-term streamflow variability in the Alps using wavelet analysis. Journal of
633 Hydrology, 587: 124927. http://dx.doi.org/10.1016/j.jhydrol.2020.124927
634 Wan Mohtar WHM, Abdullah J, Abdul Maulud KN et al. (2020) Urban flash flood
635 index based on historical rainfall events. Sustainable Cities and Society, 56:
636 102088. http://dx.doi.org/10.1016/j.scs.2020.102088
637 Wang N, Lombardo L, Tonini M et al. (2020) Implications of land use transitions and
638 climate change on local flooding in urban areas An assessment of 42 Indian cities.
639 Natural Hazards and Earth System Sciences.
640 http://dx.doi.org/10.5194/nhess-2020-238
641 Wang S, Jiao S and Xin H (2013) Spatio-temporal characteristics of temperature and
642 precipitation in Sichuan Province, Southwestern China, 1960–2009. Quaternary
643 International, 286: 103-115. http://dx.doi.org/10.1016/j.quaint.2012.04.030
644 Wang Y, Dai E, Yin L et al. (2018) Land use/land cover change and the effects on
645 ecosystem services in the Hengduan Mountain region, China. Ecosystem Services,
646 34: 55-67. http://dx.doi.org/10.1016/j.ecoser.2018.09.008
647 Wu S, Pan T, Liu Y et al. (2017) Comprehensive climate change risk regionalization
648 of China. Acta Geographica Sinica, 72(1): 3-17.
649 http://dx.doi.org/10.11821/dlxb201701001
650 Xiong J, Li J, Cheng W et al. (2019) Spatial-temporal distribution and the influencing
651 factors of mountain flood disaster in southwest China. Acta Geographica Sinica,
652 74(7): 1374-1391. http://dx.doi.org/10.11821/dlxb201907008

653 Xu F, Jia y, Niu C et al. (2018) Variation Character of Annual, Seasonal and Monthly
654 Temperature and Precipitation. Mountain Resarch, 36(2): 171-183.
655 Yang W, Liu Y, He T et al. (2020) Spatial and temporal patterns of NPP and its
656 response to climate change in the Qinghai-Tibet Plateau from 2000 to 2015.
657 Journal of Natural Resources, 35(10): 2511-2527.
658 http://dx.doi.org/10.31497/zrzyxb.20201016
659 Yin J, Gentine P, Zhou S et al. (2018) Large increase in global storm runoff extremes
660 driven by climate and anthropogenic changes. Nat Commun, 9(1): 4389.
661 http://dx.doi.org/10.1038/s41467-018-06765-2
662 Yin L, Dai E, Zheng D et al. (2020) What drives the vegetation dynamics in the
663 Hengduan Mountain region, southwest China: Climate change or human activity?
664 Ecological Indicators, 112: 106013.
665 http://dx.doi.org/10.1016/j.ecolind.2019.106013
666 Yu H, Wang L, Yang R et al. (2018a) Temporal and spatial variation of precipitation in
667 the Hengduan Mountains region in China and its relationship with elevation and
668 latitude. Atmospheric Research, 213: 1-16.
669 http://dx.doi.org/10.1016/j.atmosres.2018.05.025
670 Yu L, Xu Y and Zhang Y (2018b) Temporal and spatial variation of rainstorms and the
671 impact of flood disasters due to rainstorm in China in the past 25 years. Torrential
672 Rain and Disasters 37(1): 67-72.
673 http://dx.doi.org/10.3969/j.issn.1004-9045.2018.01.009
674 Yuan X, Liu Y, Huang Y et al. (2017) An approach to quality validation of large-scale

675 data from the Chinese Flash Flood Survey and Evaluation (CFFSE). Natural
676 Hazards, 89(2): 693-704. http://dx.doi.org/10.1007/s11069-017-2986-0
677 Yue Q, Zhang L, Liu C et al. (2016) Sensitivity of flood disaster to land use types in
678 upstream of Ganjiang Rvier. Bulletin of soil and water conservation, 36(4): 16-21.
679 Zhang G, Cui P, Jin W et al. (2021a) Changes in hydrological behaviours triggered by
680 earthquake disturbance in a mountainous watershed. Sci Total Environ, 760:
681 143349. http://dx.doi.org/10.1016/j.scitotenv.2020.143349
682 Zhang G, Cui P, Yin Y et al. (2019a) Real-time monitoring and estimation of the
683 discharge of flash floods in a steep mountain catchment. Hydrological Processes,
684 33(25): 3195-3212. http://dx.doi.org/10.1002/hyp.13551
685 Zhang K, Pan S, Cao L et al. (2014) Spatial distribution and temporal trends in
686 precipitation extremes over the Hengduan Mountains region, China, from 1961 to
687 2012. Quaternary International, 349: 346-356.
688 http://dx.doi.org/10.1016/j.quaint.2014.04.050
689 Zhang L, Nan Z, Yu W et al. (2018) Comparison of baseline period choices for
690 separating climate and land use/land cover change impacts on watershed
691 hydrology using distributed hydrological models. Sci Total Environ, 622-623:
692 1016-1028. http://dx.doi.org/10.1016/j.scitotenv.2017.12.055
693 Zhang Y, Wang Y, Chen Y et al. (2019b) Assessment of future flash flood inundations
694 in coastal regions under climate change scenarios-A case study of Hadahe River
695 basin in northeastern China. Sci Total Environ, 693: 133550.
696 http://dx.doi.org/10.1016/j.scitotenv.2019.07.356

697 Zhang Y, Wang Y, Chen Y et al. (2021b) Projection of changes in flash flood
698 occurrence under climate change at tourist attractions. Journal of Hydrology, 595:
699 126039. http://dx.doi.org/10.1016/j.jhydrol.2021.126039
700 Zhou C, Cen S, Li Y et al. (2011) Precipitation Variation and Its Impacts in Sichuan in
701 the Last 50 Years. Acta Geographica Sinica, 66(5): 619-630.
702

Figures

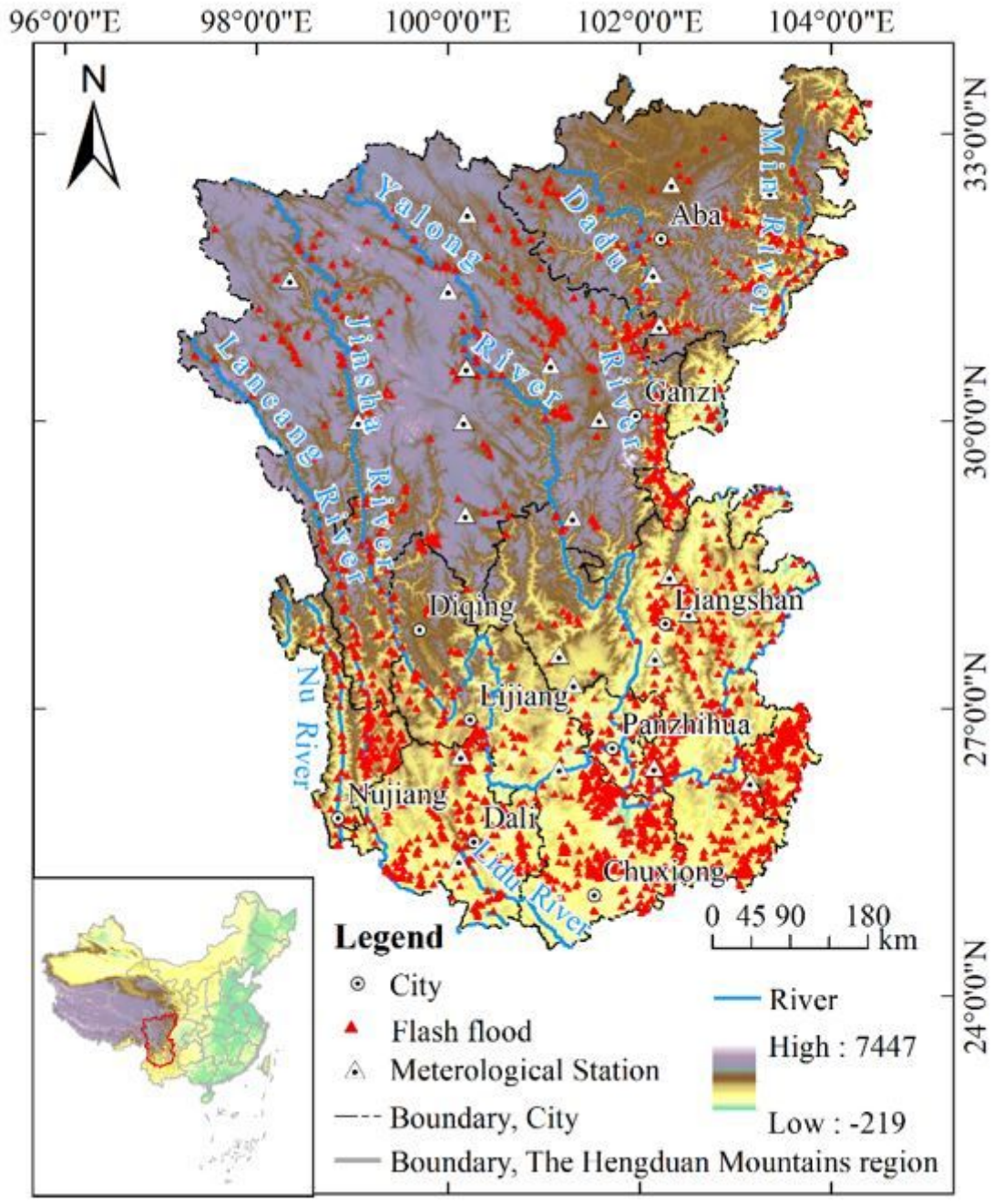

Figure 1

The HMR with meteorological stations and locations of flash flood events Note: The designations employed and the presentation of the material on this map do not imply the expression of any opinion whatsoever on the part of Research Square concerning the legal status of any country, territory, city or area or of its authorities, or concerning the delimitation of its frontiers or boundaries. This map has been provided by the authors.

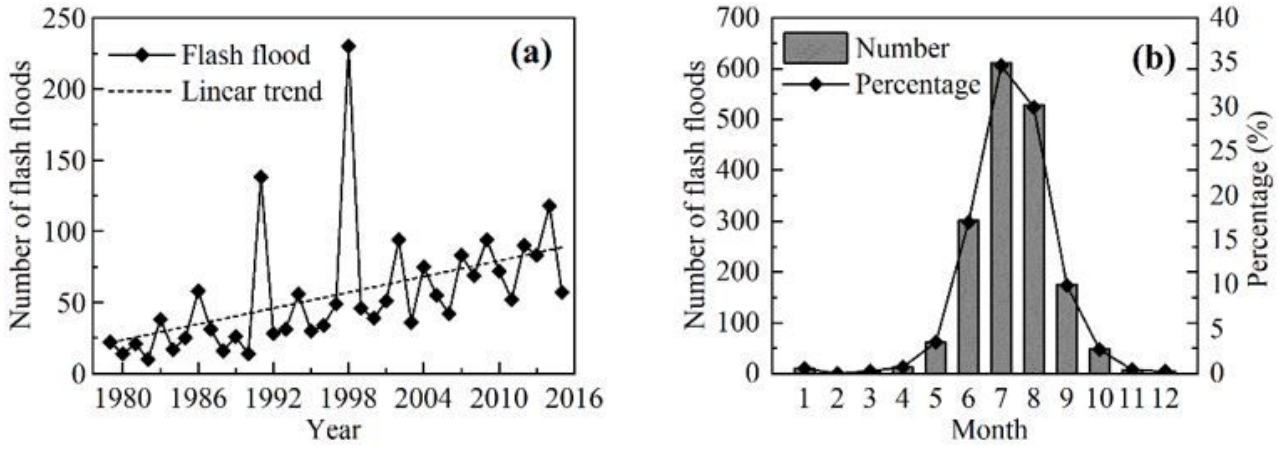

Figure 2

The statistically annual variation (a) and monthly distribution (b) of flash floods in the HMR during 1979-2015

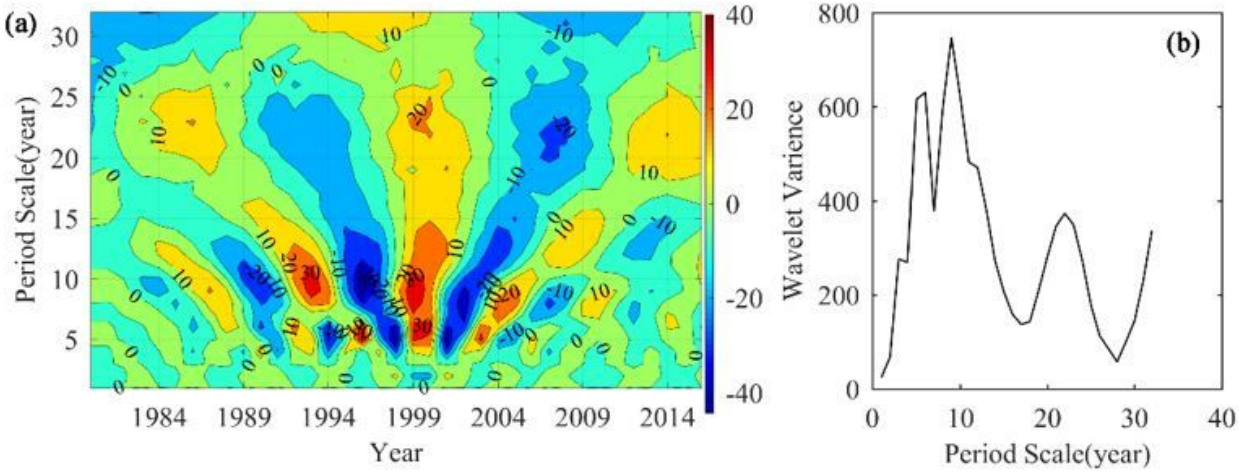

Figure 3

Distribution of time frequencies on the real part of wavelet transform (a) and the wavelet variances (b) in flash floods in the HMR during 1979-2015 Note: The designations employed and the presentation of the material on this map do not imply the expression of any opinion whatsoever on the part of Research Square concerning the legal status of any country, territory, city or area or of its authorities, or concerning the delimitation of its frontiers or boundaries. This map has been provided by the authors.

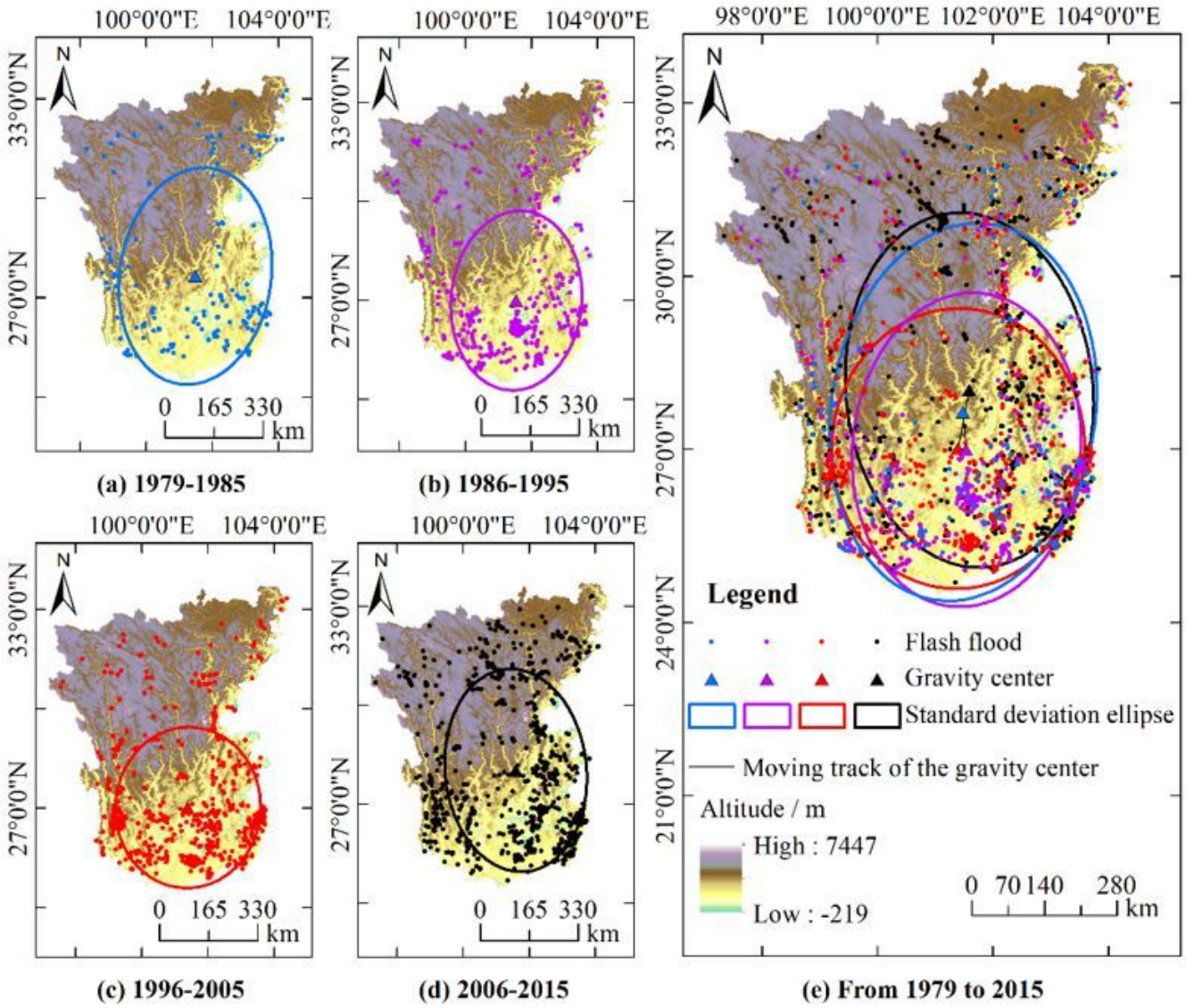

Figure 4

Gravity Center and Directional Distribution of flash floods from 1979 to 2015 Note: The designations employed and the presentation of the material on this map do not imply the expression of any opinion whatsoever on the part of Research Square concerning the legal status of any country, territory, city or area or of its authorities, or concerning the delimitation of its frontiers or boundaries. This map has been provided by the authors.

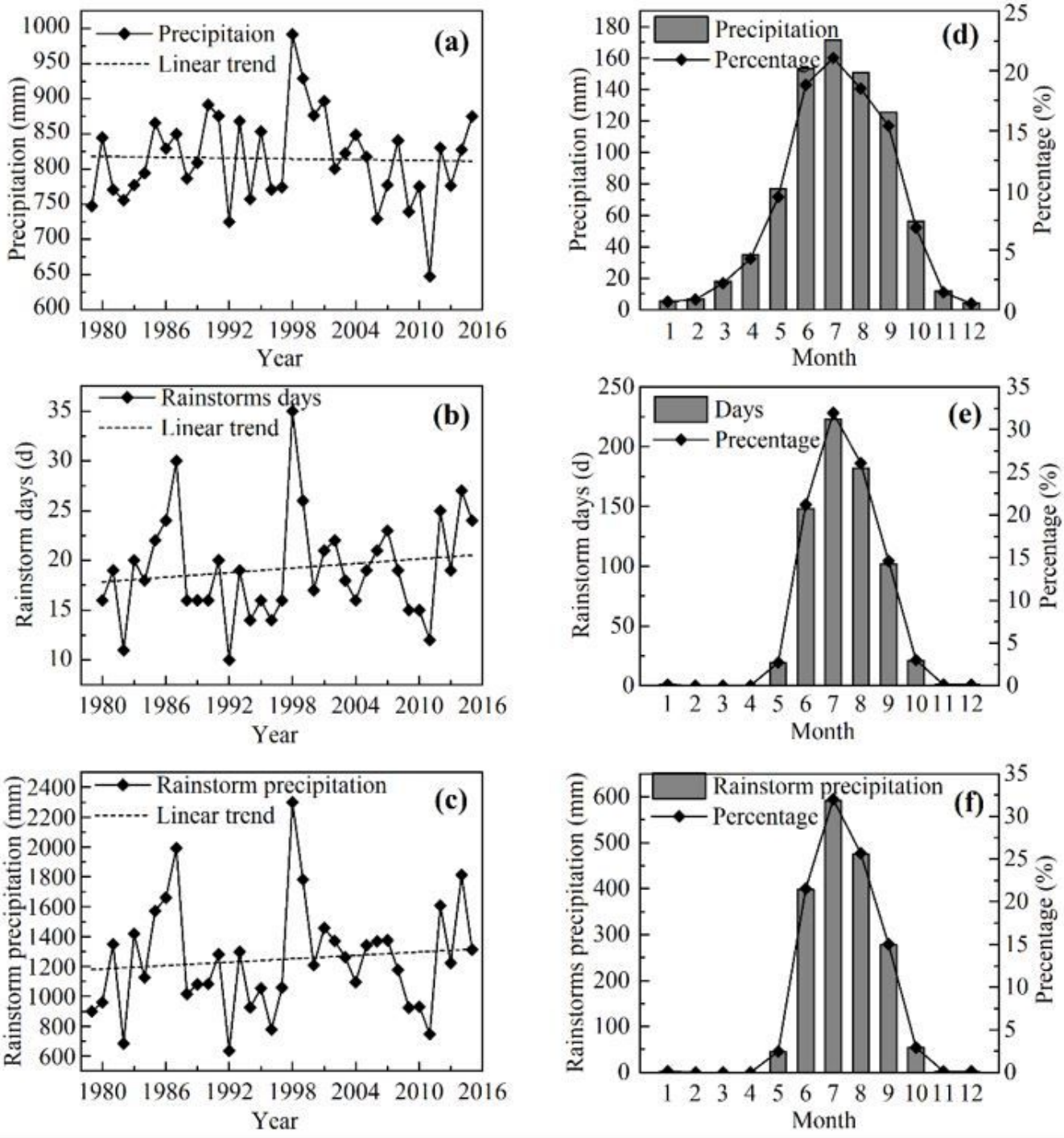

Figure 5

Annual evolution (a, b, c) and monthly distribution (d, e, f) of the rainfall (unit: mm), the rainstorm days (unit: d), and the rainstorms precipitation (unit: mm) in the HMR from 1979 to 2015.

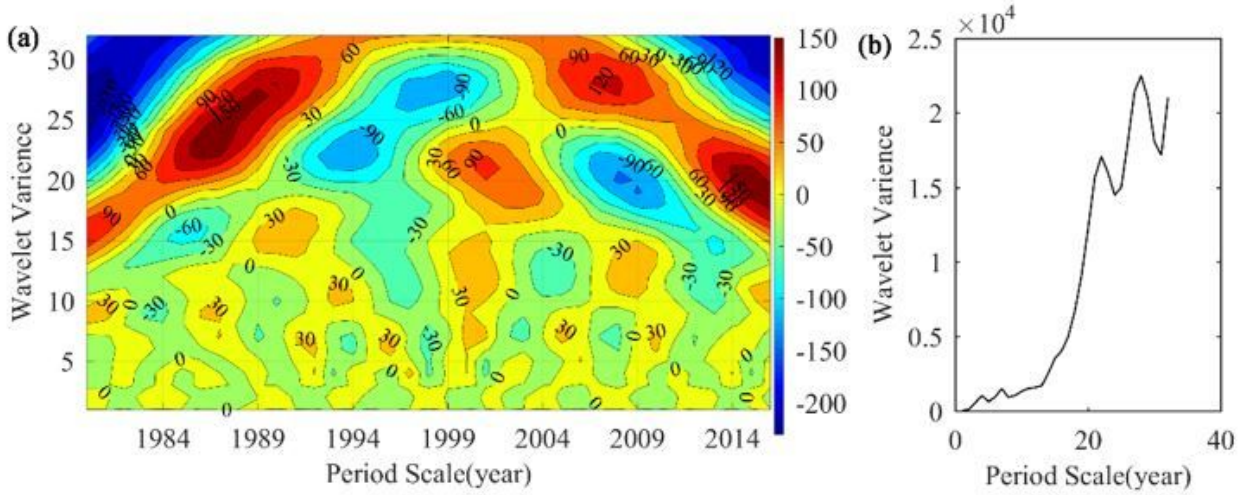

Figure 6

Distribution of time frequencies on the real part of wavelet transform (a) and the wavelet variances (b) in precipitations in the HMR during 1979-2015 Note: The designations employed and the presentation of the material on this map do not imply the expression of any opinion whatsoever on the part of Research Square concerning the legal status of any country, territory, city or area or of its authorities, or concerning the delimitation of its frontiers or boundaries. This map has been provided by the authors.

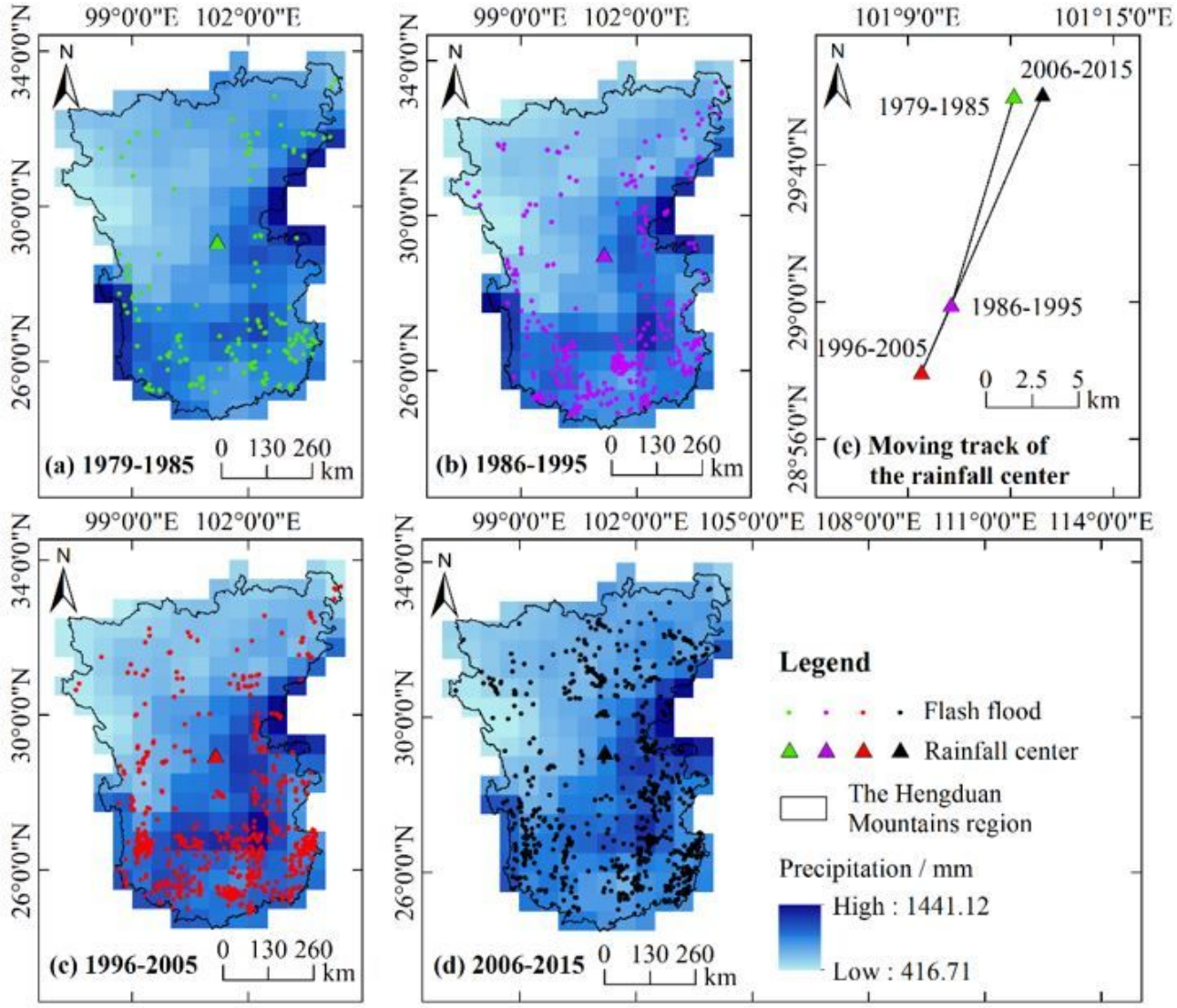

Figure 7

Moving track of the rainfall center (1979-2015) Note: The designations employed and the presentation of the material on this map do not imply the expression of any opinion whatsoever on the part of Research Square concerning the legal status of any country, territory, city or area or of its authorities, or concerning the delimitation of its frontiers or boundaries. This map has been provided by the authors.

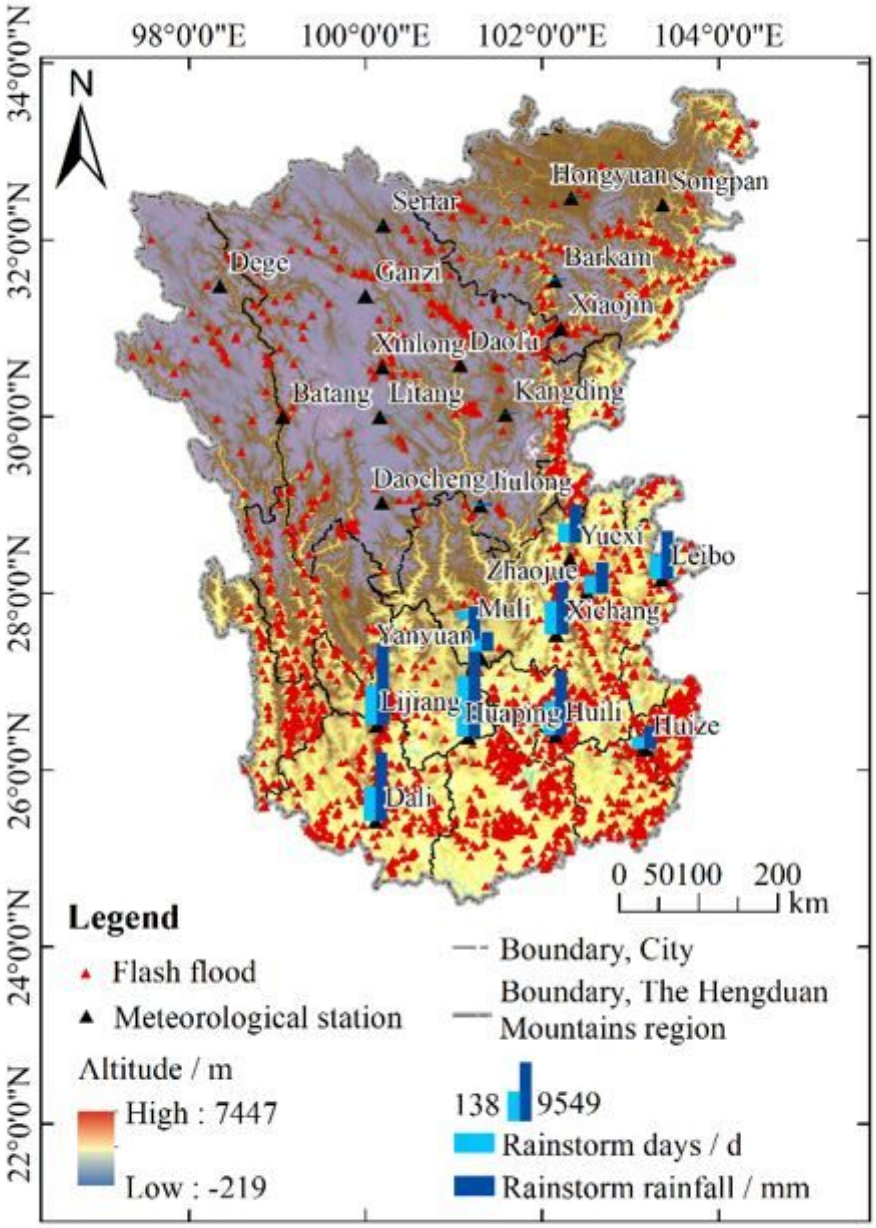

Figure 8

Distribution of the rainstorm days and rainstorm precipitation in meteorological stations in the HMR (1979-2015) Note: The designations employed and the presentation of the material on this map do not imply the expression of any opinion whatsoever on the part of Research Square concerning the legal status of any country, territory, city or area or of its authorities, or concerning the delimitation of its frontiers or boundaries. This map has been provided by the authors.

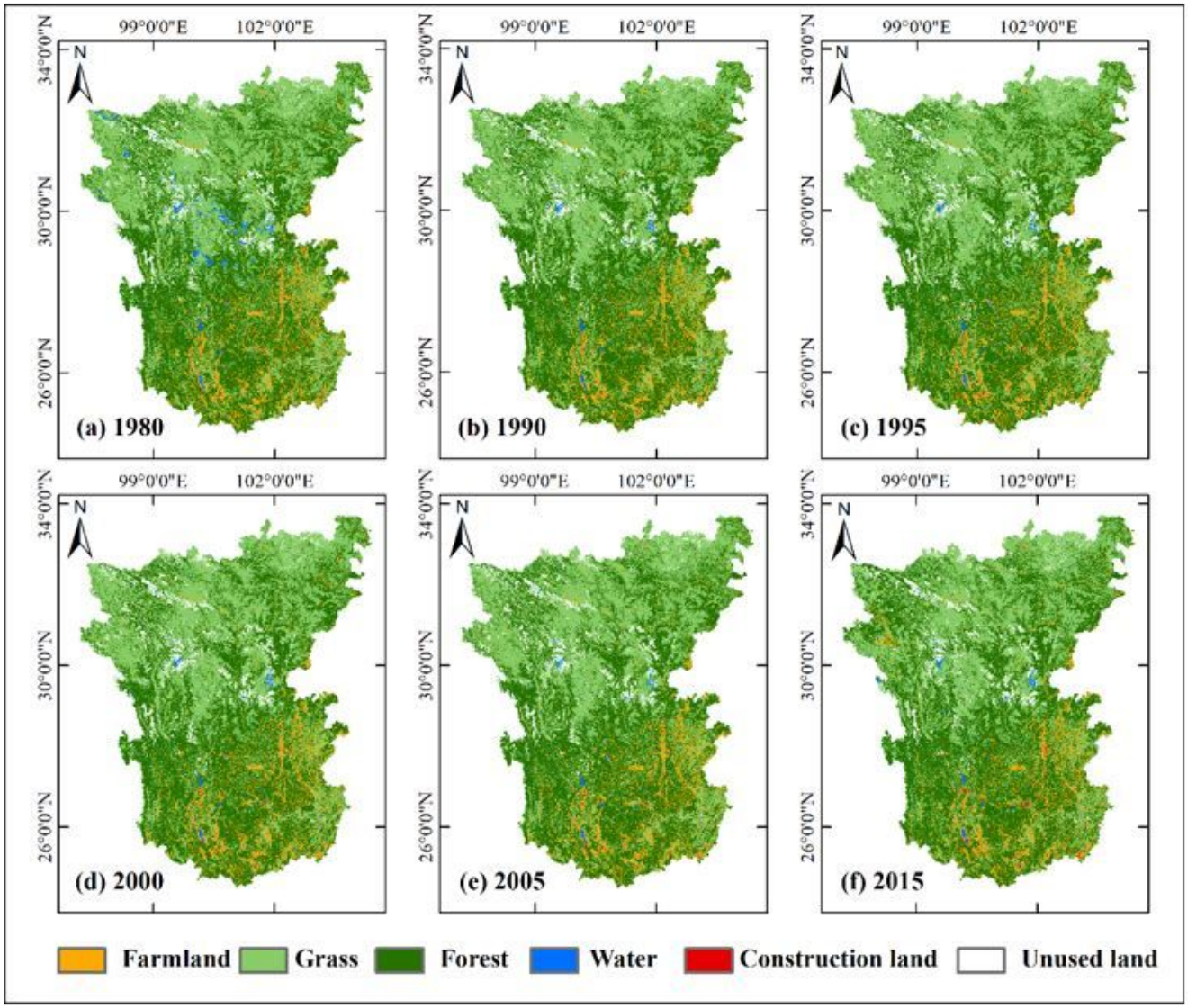

Figure 9

The land-use maps in the HMR from 1980 to 2015 (km2) Note: The designations employed and the presentation of the material on this map do not imply the expression of any opinion whatsoever on the part of Research Square concerning the legal status of any country, territory, city or area or of its authorities, or concerning the delimitation of its frontiers or boundaries. This map has been provided by the authors.

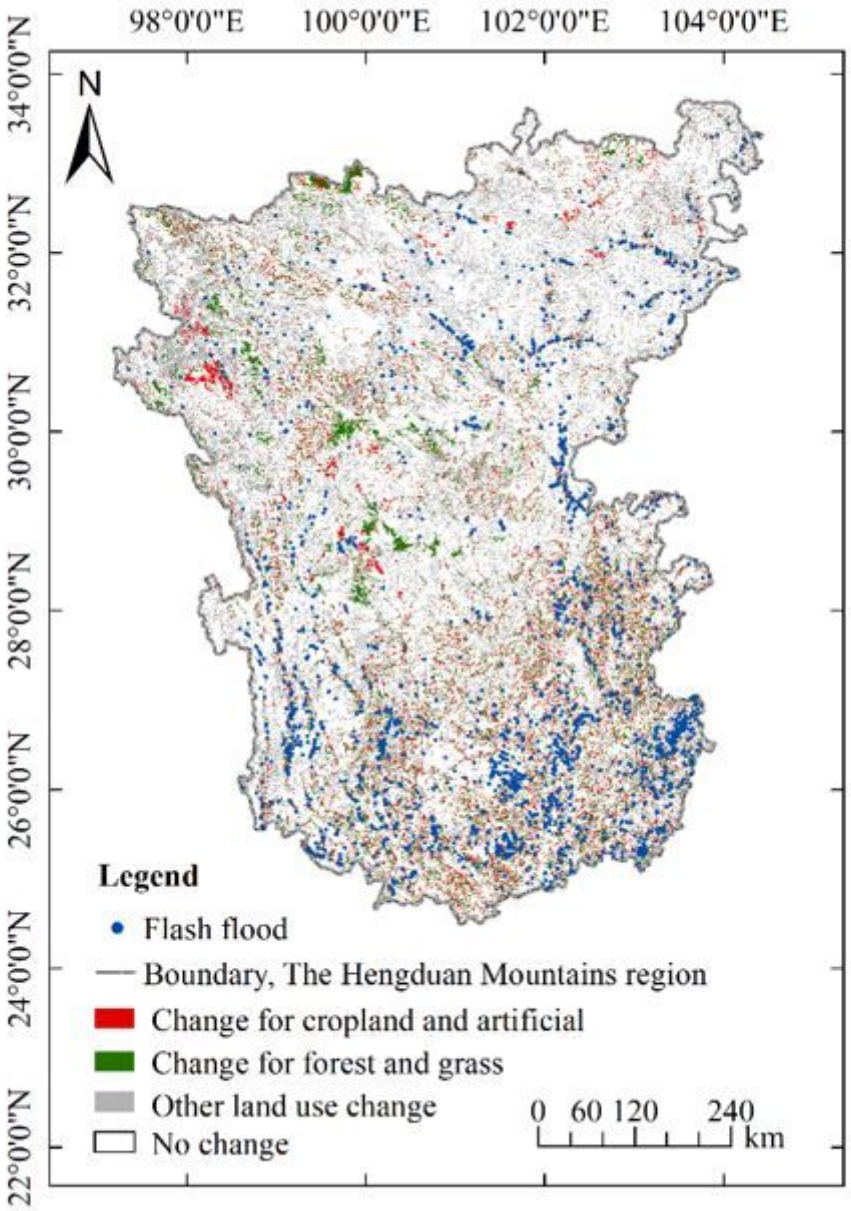

Figure 10

Distribution of land-use transfer from 1980 to 2015 Note: The designations employed and the presentation of the material on this map do not imply the expression of any opinion whatsoever on the part of Research Square concerning the legal status of any country, territory, city or area or of its authorities, or concerning the delimitation of its frontiers or boundaries. This map has been provided by the authors.

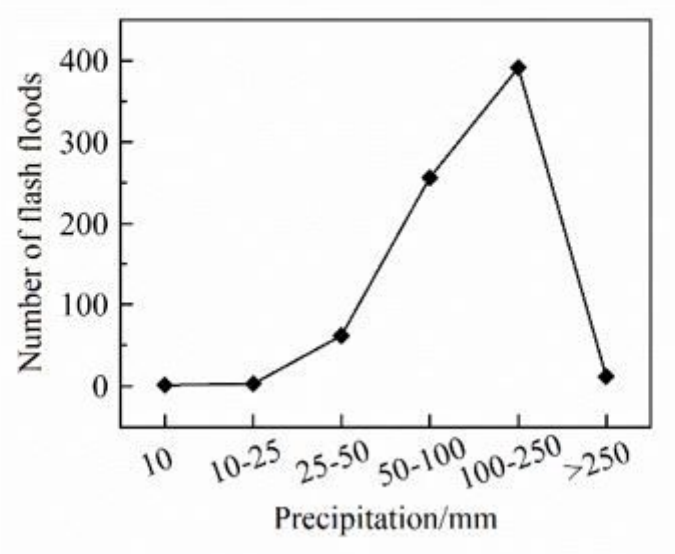

Figure 11

Number of flash floods under different rainfall grades